^{77}Se nuclear magnetic resonance of topological insulator Bi_2Se_3

Nataliya M. Georgieva,[1] Damian Rybicki,[1,2] Robin Guehne,[1] Grant V. M. Williams,[3] Shen V. Chong,[4] Kazuo Kadowaki,[5] Ion Garate,[6] and Jürgen Haase[1]

[1]*Faculty of Physics and Earth Sciences, University of Leipzig, Linnéstrasse 5, 04103 Leipzig, Germany*

[2]*Faculty of Physics and Applied Computer Science, AGH University of Science and Technology, Department of Solid State Physics, al. A. Mickiewicza 30, 30-059 Krakow, Poland*

[3]*School of Chemical and Physical Sciences, Victoria University of Wellington, PO Box 600, Wellington 6140, New Zealand*

[4]*Robinson Research Institute, Victoria University of Wellington, PO Box 33436, Lower Hutt 5046, New Zealand*

[5]*Division of Materials Science, Faculty of Pure and Applied Sciences, University of Tsukuba, 1-1-1, Tennodai, Tsukuba, Ibaraki 305-8573, Japan*

[6]*Département de Physique and Regroupement Québécois sur les Matériaux de Pointe, Université de Sherbrooke, Sherbrooke, Québec, Canada J1K 2R1*

(Received 31 October 2015; revised manuscript received 23 April 2016; published 11 May 2016)

Topological insulators constitute a new class of materials with an energy gap in the bulk and peculiar metallic states on the surface. We report on new features resulting from the *bulk* electronic structure, based on a comprehensive nuclear magnetic resonance (NMR) study of ^{77}Se on Bi_2Se_3 and $Cu_{0.15}Bi_2Se_3$ single crystals. First, we find two resonance lines and show that they originate from the two inequivalent Se lattice sites. Second, we observe unusual field-independent linewidths and attribute them to an unexpectedly strong internuclear coupling mediated by bulk electrons. In order to support this interpretation, we present a model calculation of the indirect internuclear coupling and show that the Bloembergen-Rowland coupling is much stronger than the Ruderman-Kittel-Kasuya-Yosida coupling. Our results call for a revision of earlier NMR studies and add information concerning the bulk electronic properties.

DOI: 10.1103/PhysRevB.93.195120

I. INTRODUCTION

The discovery of topological phases of matter in three dimensions has sparked great interest in the scientific community [1,2]. Three-dimensional topological insulators (TIs) were predicted [3–6] and subsequently confirmed [7–10] in spin-orbit coupled systems with inverted band structures. Among these, Bi_2Se_3 has emerged as a model system due to its simple surface states and due to the relative ease with which it can be synthesized in the form of large single crystals. The crystal structure of Bi_2Se_3 consists of stacked, van der Waals bonded quintuple layers (QL) of five atomic sheets each, with the c axis normal to the layers, cf. Fig. 1(a). Each QL contains two equivalent "outer" Se atoms (Se_{out}), two equivalent Bi atoms, and another "inner" Se atom (Se_{in}) located at the center of inversion (the unit cell comprises 3 QL) [6]. In spite of its energy gap, the bulk of Bi_2Se_3 is conducting due to self-doping with electrons from Se vacancies, with carrier concentration (n) ranging from 2×10^{17} to 2×10^{19} cm^{-3} [11–14], which can be increased, e.g., by intercalation of Cu [15–17].

NMR is a powerful probe of chemical and electronic material properties. Although NMR parameters such as shifts, linewidths, relaxation are sensitive to the electronic structure, e.g., through the local spin and orbital susceptibilities, it is unclear what NMR can contribute to the understanding of the topological surface states or to any special bulk properties of TIs (note, however, that NMR has been proposed [18] as a probe of the pairing symmetry in topological superconductors). So far, there have been few NMR studies of TIs: ^{209}Bi NMR of Bi_2Se_3 single crystals and powders [14,19–21], ^{125}Te NMR of Bi_2Te_3 [22–25], and ^{77}Se NMR of Bi_2Se_3 powder [22]. While all of these confirm bulk conductivity qualitatively from fast longitudinal nuclear relaxation ($1/T_1$), they leave many questions unanswered. For example, although the two inequivalent Se (nuclear spin $I = 1/2$) or Te ($I = 1/2$) sites should give rise to different NMR signals, they have not been found or discussed, while signals from surface states have been invoked [23,25]. Even where reported, special line shapes or spin echo behaviors are not understood, e.g., for ^{209}Bi NMR ($I = 9/2$) [14,19,20], pointing to unusual electronic properties. Therefore, understanding the NMR of TIs opens up the possibility of a more detailed comprehension of these materials, which will ultimately help in a NMR-based characterization of surface states.

Herein, we report on mostly ^{77}Se NMR studies of Bi_2Se_3 and $Cu_{0.15}Bi_2Se_3$. We identify two bulk Se signals that we prove to be due to Se_{in} and Se_{out}. We find NMR shifts, relaxation, linewidths, and spin echo decays to be quite

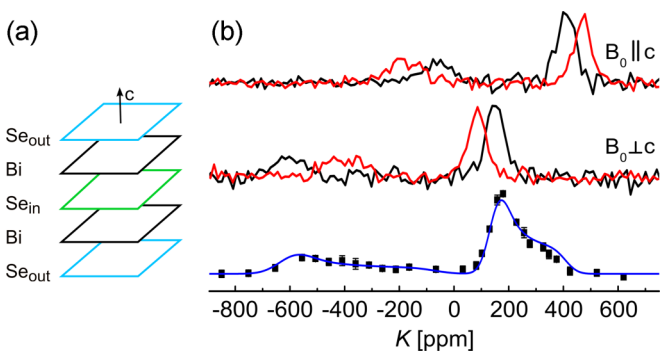

FIG. 1. (a) Sketch of the quintuple layer. (b) ^{77}Se NMR spectra at $B_0 = 17.6$ T and room temperature of Bi_2Se_3 (black) and $Cu_{0.15}Bi_2Se_3$ (red) single crystals for two crystal orientations (top two), and of Bi_2Se_3 powder (squares) with simulation based on single crystal data (solid blue line). Shifts (K) are given with respect to $(CH_3)_2Se$.

different at these two sites. We discover a strong indirect internuclear coupling that is mediated by the bulk electrons and that is responsible for the unusual linewidths and echo decays of ^{77}Se (probably also for ^{209}Bi NMR). Moreover, our model theoretical calculations show that the indirect internuclear coupling is dominated by the Bloembergen-Rowland (BR), as opposed to the Ruderman-Kittel-Kasuya-Yosida (RKKY), mechanism. This unexpected finding is related to the enhanced interband (Van Vleck) spin susceptibility predicted earlier in certain topological materials [26], and has implications, e.g., for the carrier-mediated ferromagnetism in magnetically-doped topological insulators [27]. Thus, our results give insight into the electronic properties of Bi_2Se_3, call for a revision of conclusions from earlier NMR studies, and help lay a foundation for the characterization of surface states with NMR.

II. EXPERIMENTAL DETAILS

Single crystals of Bi_2Se_3 and $Cu_{0.15}Bi_2Se_3$ have been grown as described in Ref. [28]. Granular Bi_2Se_3 from Sigma Aldrich was ground to a fine powder prior to experiments. ^{77}Se NMR was studied at $B_0 = 7$, 11.7, and 17.6 Tesla with standard wide-bore NMR magnets, home-built probes, and commercial consoles. The signals were acquired with spin echo pulse sequences $(\pi/2 - \tau - \pi)$ with typical $\pi/2$ pulse lengths of 5 to 7 μs. Each of the single crystal signals was excited separately, for the powder spectrum frequency stepped excitation was used. T_1 was determined using saturation recovery. ^{77}Se has a low natural abundance (7.63%); accordingly, even at the highest field about 2000 scans were necessary to obtain a sufficient signal-to-noise ratio. We have found the radio frequency (RF) tank circuits' quality factors ($Q = \omega L/r$) determined by losses from single crystals with changes of the apparent series resistance (r) rather than the inductance (L) [29]. Typical quality factors were $Q \approx 30$. We also estimated the absolute NMR intensities for the single crystal samples, i.e., the number of observed nuclei. For calibration we used H_2SeO_3 powder with the same RF coil, and we corrected for differences in the quality factor and spin echo decay ($1/T_{2G}$). We find that at least 25% of the ^{77}Se nuclei contribute to the signal. This corresponds to an RF penetration depth of at least 80 μm in $Cu_{0.15}Bi_2Se_3$ (resistivity data [15] gives 100 μm at 200 K for a $Cu_{0.12}Bi_2Se_3$ sample with $n = 2\times10^{20}$ cm^{-3}).

III. EXPERIMENTAL RESULTS

Typical ^{77}Se NMR spectra are shown in the upper part of Fig. 1(b). We identify two resonance lines, a narrower and a wider signal, with an intensity ratio of about 2:1. The spectrum of the Cu doped sample is similar to that of Bi_2Se_3, except for differences in the shifts. All signals are Gaussian functions of time, i.e., with the form $\exp\{-t^2/2T_{2G}^{*2}\}$. The T_1 for both signals is a few seconds in Bi_2Se_3, but an order of magnitude smaller in the Cu doped sample, see Table I. The powder spectrum of Bi_2Se_3 in the bottom of Fig. 1(b) consists of two regions (with an intensity ratio of about 2:1), in agreement with what we calculate from our single crystal data.

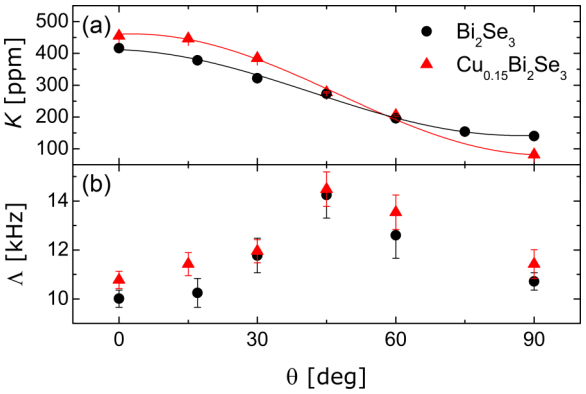

FIG. 2. Angular dependences of shifts K (a) and linewidths $\Lambda = \sqrt{\ln 4}/(\pi T_{2G}^*)$ (b) of Se_{out} in Bi_2Se_3 and $Cu_{0.15}Bi_2Se_3$ single crystals at 17.6 T. The solid lines in (a) are fits to $K = K_{iso} + \Delta K\,(3\cos^2\theta - 1)/2$.

Figure 2 depicts the dependence of the shifts and linewidths on the polar angle θ (between the crystal c axis and the magnetic field B_0) for the narrow lines. These findings are in agreement with the crystal structure. However, we estimate ^{77}Se NMR linewidths from magnetic dipole interaction [30] to be 0.7 kHz (1.3 kHz) for Se_{out} and 0.6 kHz (1.6 kHz) for Se_{in}, with $B_0 \parallel c$ ($B_0 \perp c$), while the experimental widths are an order of magnitude larger and with a much weaker angular dependence, cf. Table I.

Typical spin echo decays are shown in Fig. 3(a). The Gaussian decay constants (T_{2G}) range between 95 and 260 μs for Bi_2Se_3 and are all shortened in $Cu_{0.15}Bi_2Se_3$ by about a factor 2.4, cf. Table I. We estimate decay constants between 2300 and 4800 μs from homonuclear dipolar coupling between similar ^{77}Se nuclei [30].

Given the discrepancies between measured and expected linewidths as well as echo decays, we have investigated the magnetic field dependence of the linewidths. The results are shown in Fig. 3(b). Surprisingly, we find large field-*independent* linewidths, i.e., about 9 kHz for Se_{out} and 24 kHz

TABLE I. Measured total shift K, spin-lattice relaxation time T_1, linewidth Λ and spin echo decay time T_{2G} in Bi_2Se_3 and $Cu_{0.15}Bi_2Se_3$ at ambient conditions and 17.6 T.

Bi_2Se_3	Bi_2Se_3				$Cu_{0.15}Bi_2Se_3$			
	K [ppm]	T_1 [s]	Λ [kHz]	T_{2G} [μs]	K [ppm]	T_1 [s]	Λ [kHz]	T_{2G} [μs]
$B_0 \parallel c$, Se_{out}	410 ± 7	4.7 ± 0.3	10.1 ± 0.4	260 ± 20	475 ± 5	0.40 ± 0.03	10.8 ± 0.4	113 ± 4
$B_0 \parallel c$, Se_{in}	−63 ± 7	1.4 ± 0.3	24.0 ± 0.7	134 ± 2	−175 ± 10	0.13 ± 0.01	20.6 ± 1.2	54 ± 2
$B_0 \perp c$, Se_{out}	144 ± 7	3.0 ± 0.3	10.9 ± 0.1	215 ± 10	86 ± 15	0.21 ± 0.02	12.4 ± 1.2	99 ± 5
$B_0 \perp c$, Se_{in}	−605 ± 12	2.0 ± 0.3	24.3 ± 0.7	95 ± 10	−400 ± 10	0.24 ± 0.03	24.7 ± 3.5	35 ± 5

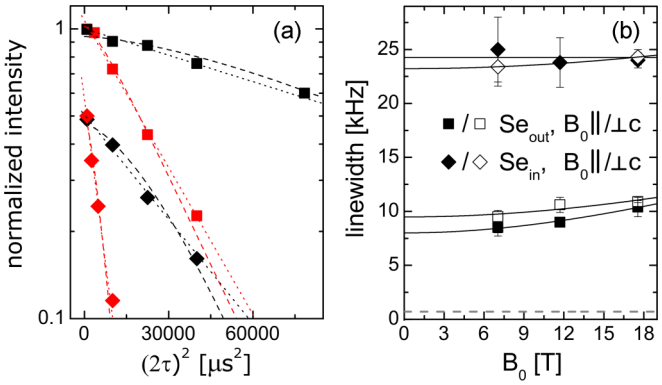

FIG. 3. (a) Bi_2Se_3 (black) and $Cu_{0.15}Bi_2Se_3$ (red), spin echo decays of Se_{out} (squares) and Se_{in} (diamonds) at 17.6 T for $B_0 \parallel c$. Dotted lines are Gaussian fits proportional to $\exp\{-(2\tau)^2/2T_{2G}^2\}$. Dashed lines are Recchia fits (see text) with second moments taken from the field-independent linewidths in Bi_2Se_3 from (b). (b) Bi_2Se_3, linewidths (Λ) of Se_{out} and Se_{in} at different magnetic fields B_0. Solid lines are fits to $\Lambda^2 = \Lambda_0^2 + [bB_0]^2$, the dashed line represents the maximal linewidth expected from magnetic dipole interaction (see text).

for Se_{in}, while the field-dependent linewidths are less than ∼50 ppm (0.4 kHz/T).

IV. DISCUSSION

We will now discuss our observations. Clearly, the two ^{77}Se NMR signals originate from the outer (Se_{out}) and inner (Se_{in}) sites of the QL, because (i) an intensity ratio of 2:1 is expected from stoichiometry, (ii) we observe the bulk of all samples, and (iii) the powder spectrum with much higher surface area is in agreement with single crystal data. The powder spectrum reported in Ref. [22] could not distinguish the two signals due to the large field-independent linewidths and the low applied magnetic field (7.05 T). In the supplement of Ref. [21], a single crystal ^{77}Se NMR spectrum consisting of one line with a field-independent ∼12 kHz linewidth is reported. This suggests the authors observed only Se_{out}, while Se_{in} was missing, probably due to noise. Since Bi_2Te_3 is structurally similar to Bi_2Se_3, we anticipate the existence of two bulk Te signals therein. In fact, a ^{125}Te NMR single crystal spectrum consisting of two resonances (a broader weaker one at approximately −600 ppm and a narrower stronger one at +400 ppm) has been reported in Ref. [25], but ascribed to surface and bulk states. In view of our results, this interpretation and some related explanations [22,23] based on ^{125}Te NMR should be revised.

Next, we address the shift and relaxation data. The relatively short T_1 of ^{77}Se (spin-1/2) in Bi_2Se_3, cf. Table I, demands a significant Fermi level density of states (DOS) in the bulk of the material. This is supported by our preliminary ^{209}Bi NMR results, which give $^{209}T_1 \sim 10$ ms in Bi_2Se_3 (data not shown), in agreement with Refs. [14,19]. Doping with Cu shortens the T_1 of ^{77}Se by about a factor of 10, likely due to an increase in DOS. Hence, we expect the shift in Bi_2Se_3 and $Cu_{0.15}Bi_2Se_3$ to consist of chemical and Knight shift contributions, the latter being larger for $Cu_{0.15}Bi_2Se_3$. Assuming that the chemical shift does not depend on doping, we interpret the shift differences between both materials by a change in Knight shift. For the change in the isotropic Knight shift, i.e., $K_{iso}(Cu_{0.15}Bi_2Se_3) - K_{iso}(Bi_2Se_3)$, we find −17 ppm ($Se_{out}$) and +99 ppm ($Se_{in}$) (cf. Table I and note that $K_{iso} = (K_\parallel + 2K_\perp)/3$). Possible contributors to the isotropic Knight shift are the Fermi contact hyperfine term and the core polarization (expected to make a negative contribution because an unpaired electron in the 4p shell gives approximately −5 T [31]). In the presence of spin-orbit coupling, orbital effects and dipolar interactions can also make a sizable contribution to K_{iso} [32,33]. For the Knight shift anisotropies, i.e., $\Delta K(Cu_{0.15}Bi_2Se_3) - \Delta K(Bi_2Se_3)$, we find +80 ppm ($Se_{out}$) and −210 ppm ($Se_{in}$) (with $\Delta K = 2(K_\parallel - K_\perp)/3$). In order to disentangle the different shift contributions, numerical calculations will be necessary for materials with known carrier concentration. The first attempts along this direction have been presented in Ref. [33].

For the remainder of this paper we argue that the large field-independent linewidths of both resonances are due to indirect internuclear coupling mediated by *bulk* electrons. This mechanism has not been discussed in previous NMR studies of TIs. Specifically, we argue that the Se linewidths are dominated by the indirect scalar coupling between ^{77}Se nuclei and the 100% abundant ^{209}Bi nuclei (the coupling between ^{77}Se nuclei can be neglected due to low natural abundance and small spin). We approximate the indirect scalar coupling between ^{77}Se and ^{209}Bi by a Hamiltonian $H = \sum_{ij} J_{ij}\mathbf{I}_i \cdot \mathbf{I}_j$ (i = Se, j = Bi). Then, the second moment that describes the width of a particular Se resonance line (i) is given by [30]

$$\langle \Delta\omega^2 \rangle_i = \sum_j \frac{I_j(I_j+1)}{3\hbar^2} J_{ij}^2, \qquad (1)$$

where $I_j = 9/2$ is the nuclear spin for ^{209}Bi.

Within a model calculation, the exchange coupling constants (J_{ij}) are computed using second order perturbation theory in the contact hyperfine interaction (for details, see the Appendix). A central quantity in this calculation is the local spin susceptibility of the itinerant electrons. We find that the interband part of the susceptibility, which involves transitions between the valence band and the conduction band, is strongly dominant. Consequently, the indirect internuclear coupling is of BR (rather than RKKY) type [34]. This means that the internuclear coupling is nonzero even when the Fermi level is placed inside the bulk gap, and weakly dependent on the carrier density in the low-doping regime. This result follows in part from the small band gaps of these materials (which implies a relatively long range of the BR coupling), and in part from the strong interband matrix elements of the electronic spin operator [26]. A dominant BR coupling, unusual in doped systems, should also play a role in the ordering of magnetic impurities in topological materials. Yet, although a strong BR coupling may be common in narrow-gap Dirac insulators, it is not *per se* a smoking gun of nontrivial band topology.

In Fig. 4, we plot the linewidth calculated with (1) for Se_{in}, following a model calculation for J_{ij} as a function of carrier concentration. While the density dependence of the calculated Knight shift due to contact hyperfine interaction K_{iso}^{hf} is of the order of a few hundred ppm over a density range of 10^{19} cm^{-3},

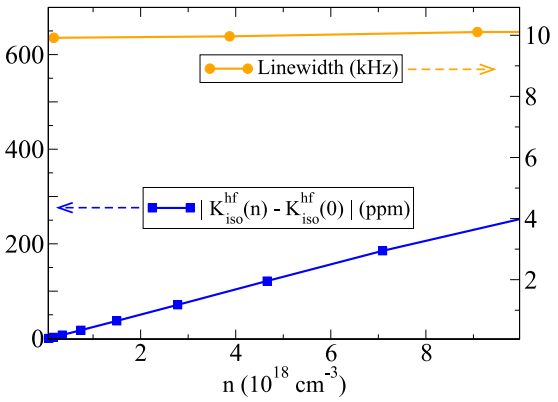

FIG. 4. Calculated isotropic n-dependent Knight shift ($|K^{\rm hf}_{\rm iso}(n) - K^{\rm hf}_{\rm iso}(0)|$, squares) and linewidth ($\sqrt{\langle\Delta\omega^2\rangle}\sqrt{\ln 4}/\pi$, bullets) as a function of the carrier density n, for Se_{in} (solid lines are guides to the eye). The model Hamiltonian and the electronic g factors are adopted from Ref. [35]. In the calculation of $|K^{\rm hf}_{\rm iso}(n) - K^{\rm hf}_{\rm iso}(0)|$, we have limited ourselves to the Fermi-surface contribution coming from the contact interaction. The value of the contact hyperfine interaction is chosen to yield a Knight shift magnitude in reasonable agreement with experiment. This same value is then used to calculate J_{ij} and thereafter the linewidth, following Eq. (1) and Ref. [36]. Additional details about the calculations can be found in the Appendix.

the linewidth is relatively weakly dependent on n, in *qualitative* agreement with the experiment (remember that $K^{\rm hf}_{\rm iso}$ is only one of the contributors to the measured total isotropic shift $K_{\rm iso}$). This theoretical result, which relates the linewidth to the Knight shift, supports the hypothesis that indirect nuclear coupling can play an important role in the NMR linewidths of TIs. Moreover, the weak dependence of the linewidth on the carrier concentration reflects the fact that the BR contribution to J_{ij} dominates over the RKKY contribution.

On the experimental side, field-*independent* linewidths in excess of what might be expected from internuclear dipole interaction for the spin-1/2 (nonquadrupolar) ^{77}Se nuclei point immediately to indirect nuclear spin coupling between ^{77}Se and ^{209}Bi. The largely isotropic linewidths that we measure support this interpretation, with differences between the two sites caused mainly by different hyperfine couplings. We find the spin echo decay constant to be much longer than the inverse linewidth for both Se signals (i.e., $T_{2G} \gg T^*_{2G} = \sqrt{\ln 4}/(\pi\Lambda)$, cf. Table I). This confirms a large inhomogeneous broadening of the ^{77}Se NMR, e.g., as given by (1). Fast sample rotation about the magic angle did not result in any significant narrowing or appearance of spinning sidebands for the Bi_2Se_3 powder (data not shown), as noticed before [22], thereby supporting the explanation in terms of indirect scalar coupling.

The question arises as to what causes the rather short spin echo decays since conventional homonuclear dipolar coupling is far too weak (of the order of several milliseconds). Note that the ratios between the T_{2G}s for one sample are very similar to the ratios between the T^*_{2G}s (cf. Table I), and hence must be determined by the hyperfine couplings. The fact that T_{2G} and T^*_{2G} are smaller for the less abundant Se_{in} suggests a larger hyperfine coupling for this site (in agreement with shifts and T_1).

Given that Cu doping decreases all T_{2G} by about a factor of 2.4, while the linewidths remain unchanged [37], the interaction causing the ^{77}Se linewidths cannot be responsible for the echo decays. With a double resonance experiment involving Se_{out} and Se_{in} we have confirmed that the ^{77}Se-^{77}Se coupling contributes only weakly to the spin echo decay [38].

It seems possible that ^{209}Bi spin flips, e.g., due to spin-lattice relaxation, will induce fluctuations of the ^{77}Se local field via the ^{77}Se-^{209}Bi indirect coupling, thereby causing spin echo decay. If we assume the amplitudes of the fluctuating fields at ^{77}Se given by the ^{77}Se-^{209}Bi indirect coupling, and hence by our field-independent linewidths, we can fit our decays to the theory of Recchia *et al.* [39], cf. Fig. 3(a). We obtain a single correlation time for each material (for both Se sites), 2.1 ± 0.3 ms in Bi_2Se_3 and 150 ± 50 μs in $Cu_{0.15}Bi_2Se_3$. The Bi_2Se_3 correlation time complies with our nonselectively excited $^{209}T_1$ value of 10 ms (the single level lifetime for $I = 9/2$ is about a factor of 10 smaller [40]). A tenfold shorter correlation time in $Cu_{0.15}Bi_2Se_3$ complies with an expected tenfold decrease in $^{209}T_1$ upon Cu doping due to the factor 10 decrease of $^{77}T_1$, cf. Table I. We conclude that the ^{209}Bi level lifetime together with the indirect coupling accounts for the spin echo decays.

A strong indirect coupling should also affect the ^{209}Bi NMR. Here, the coupling is dominated by ^{209}Bi-^{209}Bi interactions, but does not lead to exchange narrowing [30] since the local symmetry at the Bi site causes a sizable (∼140 to 170 kHz) quadrupole shift [14,19] of the ^{209}Bi nuclear levels, such that nuclear neighbors may not be able to participate in exchange if they are in different spin states. Furthermore, the quadrupole shift can vary from one nucleus to the next, due to strain caused by imperfections. As a result, the line broadening and spin echo behavior of ^{209}Bi NMR can be quite complicated and may depend on the impurity levels.

We have confirmed, with ^{209}Bi NMR on our Bi_2Se_3 single crystal, that all nine lines from quadrupole splitting have very similar yet large linewidths (Refs. [14,19], data not shown). This shows that quadrupolar broadening does not dominate the individual linewidths. In preliminary field-dependent measurements on Bi_2Se_3 powder, we find a large field-*independent* linewidth of about 44 ± 4 kHz for the ^{209}Bi central transition, in agreement with 46 ± 2 kHz measured in our single crystal at the magic angle and 9.4 Tesla. This width strongly exceeds the estimated dipolar linewidth of ∼1.5 kHz, and hence must be caused by indirect coupling.

Unusually large ^{209}Bi linewidths have been noticed in previous works [14,19–21], but indirect coupling was not invoked as a possible origin. Besides, rather fast ^{209}Bi NMR spin echo decays were observed, in particular in the central region of the spectra, but could not be explained. Interestingly, the linewidth from Ref. [14] increases with decreasing carrier concentration (larger linewidths for more homogeneous samples grown with excess Se). Most of these results appear compatible with a large indirect coupling between the ^{209}Bi nuclei in the presence of quadrupole interaction.

V. CONCLUSION

To conclude, we have presented a detailed ^{77}Se NMR study of Bi_2Se_3 and $Cu_{0.15}Bi_2Se_3$. First, we have identified and characterized the two resonances from Se_{in} and Se_{out}.

Secondly, we have measured large, field-independent NMR linewidths that suggest a strong Bloembergen-Rowland internuclear coupling mediated by bulk electrons. The latter finding may have implications for the carrier-mediated magnetism of topological materials, e.g., by anticipating bulk magnetic order even when the Fermi level lies inside the bulk gap. It will thus be interesting to determine its universality by conducting further experimental and theoretical studies in other topological materials.

ACKNOWLEDGMENTS

We acknowledge the help of F. Höfer and financial support from the University of Leipzig and the DFG within the Graduate School BuildMoNa. J.H. and N.G. thank B. Rosenow and B. Zocher for helpful discussions. I.G. thanks Québec's RQMP and Canada's NSERC for funding, Calcul Québec and Compute Canada for computer resources, and J. Quilliam for discussions.

APPENDIX: MODEL CALCULATION OF THE CONTACT KNIGHT SHIFT AND THE INDIRECT INTERNUCLEAR COUPLING

This Appendix contains a simplified model calculation for the contact Knight shift and the indirect internuclear interaction in bulk Bi_2Se_3. Our first aim is to estimate the hyperfine couplings by fitting our model calculation of the Knight shift to the experimental data. Afterwards, using these estimates, we calculate the NMR linewidth due to indirect internuclear interaction. The obtained linewidth is in reasonable agreement with experiment, which supports the hypothesis that the indirect internuclear coupling plays an important role in the measured linewidth.

1. Model

The electronic states describing the lowest conduction band and the highest valence band of Bi_2Se_3 at the Γ point ($k=0$) of the Brillouin zone are

$$\begin{aligned}\left|u_{+\frac{1}{2},\tau}\right\rangle &\simeq a_\tau|p_z,\tau,\uparrow\rangle + b_\tau|p_x+ip_y,\tau,\downarrow\rangle + c_\tau|s,\tau,\uparrow\rangle\\ \left|u_{-\frac{1}{2},\tau}\right\rangle &\simeq a_\tau^*|p_z,\tau,\downarrow\rangle + b_\tau^*|p_x-ip_y,\tau,\uparrow\rangle + c_\tau^*|s,\tau,\downarrow\rangle,\end{aligned} \tag{A1}$$

where $\pm1/2$ denotes the projection of the z component of the *total* angular momentum and τ labels two electronic orbitals, $P1$ and $P2$, with opposite parity under spatial inversion about the inner Se atom in each quintuple layer ($P1$ is even and $P2$ is odd). Also, $\uparrow$ ($\downarrow$) is the projection of the z component of the spin, $p_{x,y,z}$ are p-type atomic orbitals, and s is an s-type atomic orbital. Here, the x and y directions are parallel to the quintuple layers, whereas the z direction is perpendicular to them.

The complex numbers a_τ, b_τ, c_τ satisfy $|a_\tau|^2+|b_\tau|^2+|c_\tau|^2=1$. In Bi_2Se_3, $|a_\tau|>|b_\tau|>|c_\tau|$, since the low-energy orbitals are predominantly of p_z type and $\pm1/2$ agrees predominantly with the direction of the bare electronic spin. The coefficients b_τ scale as the ratio of the spin-orbit coupling to the crystal field splitting. Although c_τ is small, it makes the main contribution to the contact interaction between electrons and nuclei.

The bulk electronic states in the vicinity of the Γ point can be obtained from the following $\mathbf{k}\cdot\mathbf{p}$ Hamiltonian [6,35]:

$$h(\mathbf{k}) = \epsilon_{\mathbf{k}} + \mathbf{d}_{\mathbf{k}}\cdot\boldsymbol{\sigma}\tau^x + M_{\mathbf{k}}\tau^z + r_{\mathbf{k}}\tau^y, \tag{A2}$$

which is written in the basis spanned by $\{|P1,+1/2\rangle, |P1,-1/2\rangle, |P2,+1/2\rangle, |P2,-1/2\rangle\}$. In Eq. (A2), σ^i and τ^i are Pauli matrices ($i\in\{x,y,z\}$) such that $\tau^z\in\{P1,P2\}$ and $\sigma^z\in\{-1/2,+1/2\}$. Also, $\epsilon_{\mathbf{k}}=\gamma_x(k_x^2+k_y^2)+\gamma_z k_z^2$, $\mathbf{d}_{\mathbf{k}}=(v_x k_x, v_x k_y, v_z k_z - iR_2(k_+^3-k_-^3)/2)$, $M_{\mathbf{k}}=M+t_x(k_x^2+k_y^2)+t_z k_z^2$, $r_{\mathbf{k}}=-R_1(k_+^3+k_-^3)/2\tau^y$, where $k_\pm\equiv k_x\pm ik_y$. The parameter values are [35] $M=-0.28$ eV, $t_z=6.86$ eV Å^2, $t_x=44.5$ eV Å^2, $v_z=2.26$ eV Å, $v_x=3.33$ eV Å, $\gamma_z=5.74$ eV Å^2, $\gamma_x=30.4$ eVÅ^2, $R_1=50.6$ eVÅ^3, and $R_2=-113.3$ eVÅ^3. Although these band parameters are extracted from the band structure near $k=0$, below we will extrapolate Eq. (A2) to higher momenta.

2. Knight shift

The Knight shift originates from the field-induced magnetization of the itinerant carriers. This magnetization couples to the nuclear spins through the hyperfine and dipolar interactions, effectively acting as an extra magnetic field that acts on the nuclei and shifts the nuclear resonance frequency.

The exchange interaction between nuclear spins and itinerant spins can be written as

$$\mathcal{H}_{\text{en}} = \sum_{\mathbf{R}}\mathbf{I}(\mathbf{R})\cdot\int d^3\mathbf{r}\, A(\mathbf{r}-\mathbf{R})\,\mathbf{S}(\mathbf{r}), \tag{A3}$$

where $\mathbf{I}(\mathbf{R})$ is the spin operator for a nucleus located at $\mathbf{R}$, $\mathbf{S}(\mathbf{r})$ is the electronic spin density operator at position $\mathbf{r}$, and $A(\mathbf{r}-\mathbf{R})$ is the hyperfine coupling between the itinerant electron and the nucleus. Hereafter, we approximate [40] the hyperfine coupling by a short-ranged (contact) interaction,

$$A(\mathbf{r}-\mathbf{R}) = \tfrac{2}{3}\mu_0 g_s\mu_B\gamma_n\hbar\delta(\mathbf{r}-\mathbf{R}), \tag{A4}$$

where μ_0 is the magnetic permeability in vacuum, g_s is the g factor for electrons, and γ_n is the nuclear gyromagnetic ratio. Longer-range (dipolar) interactions and core polarization can also contribute to the Knight shift; we shall ignore these contributions for the purposes of our theoretical estimates. Note that $A(\mathbf{r})$ has units of energy, $\mathbf{S}(\mathbf{r})$ has units of inverse volume, and $\mathbf{I}(\mathbf{R})$ is dimensionless. Because the contact interaction involves length scales that are short compared to the size of an atom, the electronic g factor entering in Eq. (A4) must be taken to be $g_s\simeq 2$ regardless of the spin-orbit interactions that are present in the material [41]. Substituting Eq. (A4) in Eq. (A3), the latter becomes

$$\mathcal{H}_{\text{en}} = \tfrac{2}{3}\mu_0 g_s\mu_B\gamma_n\hbar\sum_{\mathbf{R}}\mathbf{I}(\mathbf{R})\cdot\mathbf{S}(\mathbf{R}). \tag{A5}$$

An external magnetic field $\mathbf{B}$ spin-polarizes the itinerant electrons. By virtue of the hyperfine interaction, this spin polarization leads to an extra magnetic field $\delta\mathbf{B}(\mathbf{R})$ felt by the nucleus:

$$\delta\mathbf{B}^{\text{hf}}(\mathbf{R}) = -\tfrac{2}{3}\mu_0 g_s\mu_B\langle\mathbf{S}(\mathbf{R})\rangle, \tag{A6}$$

where $\langle\,\rangle$ stands for the expectation value. This extra magnetic field is essentially the Knight shift. Next, we wish to relate $\langle \mathbf{S}(\mathbf{R})\rangle$ to the itinerant spin susceptibility that may be calculated using Eq. (A2).

We begin by recalling that the itinerant electron spin density is given by

$$\mathbf{S}(\mathbf{r}) = \frac{1}{V}\sum_{\mathbf{q}} e^{-i\mathbf{q}\cdot\mathbf{r}}\,\mathbf{S}(\mathbf{q});$$
$$\mathbf{S}(\mathbf{q}) = \sum_{\mathbf{k}\mathbf{k}'}\sum_{nn'}\langle\psi_{\mathbf{k}n}|\mathbf{s}\,e^{i\mathbf{q}\cdot\mathbf{r}'}|\psi_{\mathbf{k}'n'}\rangle c^{\dagger}_{\mathbf{k}n}c_{\mathbf{k}'n'}, \tag{A7}$$

where V is the volume of the crystal and $\mathbf{s}$ is the bare electronic spin operator [42], and

$$|\psi_{\mathbf{k}n}\rangle = \frac{e^{i\mathbf{k}\cdot\mathbf{r}}}{\sqrt{V}}|u_{\mathbf{k}n}\rangle \tag{A8}$$

is the Bloch eigenstate for an electron with crystal momentum $\mathbf{k}$ and an energy band label n. Likewise, $c^{\dagger}_{\mathbf{k}n}$ is an operator that creates an electron in state $|\psi_{\mathbf{k}n}\rangle$. Because of spin, $\psi_{\mathbf{k}n}(\mathbf{r}) = \langle\mathbf{r}|\psi_{\mathbf{k}n}\rangle$ is represented by a two-component spinor. In addition,

$$\langle\psi_{\mathbf{k}n}|\mathbf{s}\,e^{i\mathbf{q}\cdot\mathbf{r}'}|\psi_{\mathbf{k}'n'}\rangle = \int d^3r' e^{i\mathbf{q}\cdot\mathbf{r}'}\psi^{*}_{\mathbf{k}n}(\mathbf{r}')\,\mathbf{s}\,\psi_{\mathbf{k}'n'}(\mathbf{r}'). \tag{A9}$$

Within the $\mathbf{k}\cdot\mathbf{p}$ approximation, the eigenstates at momentum $\mathbf{k}$ may be written as

$$|\psi_{\mathbf{k}n}\rangle = \frac{e^{i\mathbf{k}\cdot\mathbf{r}}}{\sqrt{V}}\sum_{\sigma\tau}|u_{\sigma\tau}\rangle\langle u_{\sigma\tau}|u_{\mathbf{k}n}\rangle, \tag{A10}$$

where $|u_{\sigma\tau}\rangle$ ($\sigma\in\{+1/2,-1/2\}$, $\tau\in\{P1,P2\}$) are the eigenstates of the Bloch Hamiltonian at the Γ point, and the coefficients $\langle u_{\sigma\tau}|u_{\mathbf{k}n}\rangle$ are obtained directly from the diagonalization of Eq. (A2). After substituting Eq. (A10) in Eq. (A7), we arrive at

$$\mathbf{S}(\mathbf{q}) = \sum_{\mathbf{k}\mathbf{k}'}\sum_{\sigma\sigma'}\sum_{\tau\tau'}\langle\psi_{\mathbf{k}\sigma\tau}|\mathbf{s}\,e^{i\mathbf{q}\cdot\mathbf{r}}|\psi_{\mathbf{k}'\sigma'\tau'}\rangle c^{\dagger}_{\mathbf{k}\sigma\tau}c_{\mathbf{k}'\sigma'\tau'}, \tag{A11}$$

where we have used

$$c^{\dagger}_{\mathbf{k}\sigma\tau} = \sum_{n}\langle u_{\mathbf{k}n}|u_{\sigma\tau}\rangle c^{\dagger}_{\mathbf{k}n} \tag{A12}$$

and have defined

$$|\psi_{\mathbf{k}\sigma\tau}\rangle \equiv \frac{e^{i\mathbf{k}\cdot\mathbf{r}}}{\sqrt{V}}|u_{\sigma\tau}\rangle. \tag{A13}$$

Also, $c^{\dagger}_{\mathbf{k}\sigma\tau}$ is the operator that creates an electron in a state $|\psi_{\mathbf{k}\sigma\tau}\rangle$.

From Eqs. (A7) and (A11), it follows that

$$\mathbf{S}(\mathbf{r}) = \sum_{\mathbf{k}\mathbf{k}'}\sum_{\tau\tau'}\sum_{\sigma\sigma'}\psi^{*}_{\mathbf{k}\sigma\tau}(\mathbf{r})\mathbf{s}\psi_{\mathbf{k}'\sigma'\tau'}(\mathbf{r})c^{\dagger}_{\mathbf{k}\sigma\tau}c_{\mathbf{k}'\sigma'\tau'}$$
$$= \frac{1}{V}\sum_{\mathbf{k}\mathbf{k}'}e^{i(\mathbf{k}-\mathbf{k}')\cdot\mathbf{r}}\sum_{\tau\tau'}\sum_{\sigma\sigma'}u^{*}_{\sigma\tau}(\mathbf{r})\,\mathbf{s}\,u_{\sigma'\tau'}(\mathbf{r})c^{\dagger}_{\mathbf{k}\sigma\tau}c_{\mathbf{k}'\sigma'\tau'}, \tag{A14}$$

where we have used $\sum_{\mathbf{q}}\exp[i\mathbf{q}\cdot(\mathbf{r}-\mathbf{r}')] = V\delta(\mathbf{r}-\mathbf{r}')$. Accordingly, Eq. (A6) becomes

$$\delta\mathbf{B}^{\rm hf}(\mathbf{R}) = -\frac{2}{3}\mu_0 g_s\mu_B\sum_{\mathbf{q}}e^{i\mathbf{q}\cdot\mathbf{R}}$$
$$\times\frac{1}{V}\sum_{\mathbf{k}}\sum_{\sigma\sigma'}\sum_{\tau\tau'}u_{\sigma\tau}(\mathbf{R})^{*}\,\mathbf{s}u_{\sigma'\tau'}(\mathbf{R})\langle c^{\dagger}_{\mathbf{k}\sigma\tau}c_{\mathbf{k}-\mathbf{q}\sigma'\tau'}\rangle, \tag{A15}$$

where $\mathbf{R}$ denotes the nuclear position. Recognizing that only s-type atomic orbitals have a nonvanishing wave function at their nuclei, we may approximate [43]

$$u_{\sigma\tau}(\mathbf{R})^{*}\,\mathbf{s}\,u_{\sigma'\tau'}(\mathbf{R}) \simeq c^{*}_{\tau}(\mathbf{R})c_{\tau'}(\mathbf{R})\langle s,\tau|\mathbf{R}\rangle\langle\mathbf{R}|s,\tau'\rangle\mathbf{j}_{\sigma\sigma'}, \tag{A16}$$

where $\mathbf{j}$ is the total angular momentum operator [$(j_z)_{\sigma\sigma'} = \sigma\delta_{\sigma\sigma'}$, $(j_x)_{\sigma\sigma'} = \delta_{\sigma,-\sigma'}$, $(j_y)_{\sigma\sigma'} = -i\sigma\delta_{\sigma,-\sigma'}$]. Then,

$$\delta\mathbf{B}^{\rm hf}(\mathbf{R}) = -\frac{2}{3}\mu_0 g_s\mu_B\sum_{\mathbf{q}}e^{i\mathbf{q}\cdot\mathbf{R}}$$
$$\times\sum_{\tau\tau'}c^{*}_{\tau}(\mathbf{R})c_{\tau'}(\mathbf{R})\langle s,\tau|\mathbf{R}\rangle\langle\mathbf{R}|s,\tau'\rangle$$
$$\times\frac{1}{V}\sum_{\mathbf{k}}\sum_{\sigma\sigma'}\mathbf{j}_{\sigma\sigma'}\langle c^{\dagger}_{\mathbf{k}\sigma\tau}c_{\mathbf{k}-\mathbf{q}\sigma'\tau'}\rangle, \tag{A17}$$

where the expectation value is nonzero due to the applied magnetic field.

Let us consider a spatially uniform magnetic field $\mathbf{B}_0$. It couples to the electronic spin via

$$\mathcal{H}_Z = \mu_B\sum_{\mathbf{k}}\sum_{\tau}\frac{\mathbf{1}+\tau\tau_z}{2}\sum_{i=x,y,z}g_i(\tau)c^{\dagger}_{\mathbf{k}\sigma\tau}\,j_i\,c_{\mathbf{k}\sigma'\tau}B_i, \tag{A18}$$

where $g_i(\tau)$ is the effective g factor for orbital τ in response to the ith component of $\mathbf{B}_0$. The theoretically calculated values for $g_i(\tau)$ for Bi_2Se_3, Bi_2Te_3 and Sb_2Te_3 are tabulated in Ref. [35]. For Bi_2Se_3, $g_z(P1) = -25.4$, $g_x(P1) = g_y(P1) = -4.12$, $g_z(P2) = 4.1$ and $g_x(P2) = g_y(P2) = 4.8$. In Eq. (A18) and below, we take the convention that $1+\tau\tau^z = 1+\tau^z$ for $\tau = P1$ and $1+\tau\tau^z = 1-\tau^z$ for $\tau = P2$.

From Eq. (A18), it follows that $\langle c^{\dagger}_{\mathbf{k}\sigma\tau}c_{\mathbf{k}-\mathbf{q}\sigma'\tau}\rangle = \delta_{\mathbf{q},\mathbf{0}}\delta_{\tau\tau'}\langle c^{\dagger}_{\mathbf{k}\sigma\tau}c_{\mathbf{k}\sigma'\tau}\rangle$ and thus

$$\delta\mathbf{B}^{\rm hf}(\mathbf{R}) = -\frac{2}{3}\mu_0 g_s\mu_B\sum_{\tau}|c_\tau|^2|\langle\mathbf{R}|s,\tau\rangle|^2$$
$$\times\frac{1}{V}\sum_{\mathbf{k}}\sum_{\sigma\sigma'}\mathbf{j}_{\sigma\sigma'}\langle c^{\dagger}_{\mathbf{k}\sigma\tau}c_{\mathbf{k}\sigma'\tau}\rangle$$
$$\equiv\frac{2}{3}\mu_0 g_s\mu_B\sum_{\tau}|c_\tau|^2|\langle\mathbf{R}|s,\tau\rangle|^2\mathbf{m}(\tau), \tag{A19}$$

where $\mathbf{m}(\tau)$ is the orbitally-resolved magnetization. Hence, standard linear response theory [with Eq. (A18) as the perturbation] dictates

$$\delta B^{\rm hf}_i(\mathbf{R}) = \sum_{j\in\{x,y,z\}}K^{\rm hf}_{ij}(\mathbf{R})B_j, \tag{A20}$$

where

$$K^{\rm hf}_{ij}(\mathbf{R}) = \lambda^{\rm hf}(\mathbf{R},P1)\chi_{ij}(P1) + \lambda^{\rm hf}(\mathbf{R},P2)\chi_{ij}(P2) \tag{A21}$$

is the Knight shift tensor with only the contact contribution,

$$\lambda^{\rm hf}(\mathbf{R},\tau) \equiv \frac{2\mu_0}{3}\frac{|c_\tau|^2|\langle \mathbf{R}|s,\tau\rangle|^2}{V_{\rm mol}/N_A} \tag{A22}$$

is the orbital-dependent hyperfine coupling, $V_{\rm mol}$ is the molar volume ($\simeq 258\,{\rm cm}^3$ in Bi_2Se_3), N_A is Avogadro's number, and

$$\chi_{ij}(\tau) = \mu_B^2\frac{V_{\rm mol}}{N_A}g_s\sum_{nn'}\int\frac{d^3k}{(2\pi)^3}\langle u_{\mathbf{k}n}|j_i\frac{1+\tau\tau_z}{2}|u_{\mathbf{k}n'}\rangle \times\langle u_{\mathbf{k}n'}|j_j\left(g_j(P1)\frac{\mathbf{1}+\tau_z}{2}+g_j(P2)\frac{\mathbf{1}-\tau_z}{2}\right)|u_{\mathbf{k}n}\rangle \times\frac{f_{\mathbf{k}n}-f_{\mathbf{k}n'}}{E_{\mathbf{k}n'}-E_{\mathbf{k}n}} \tag{A23}$$

is the orbital-resolved molar spin susceptibility. In Eq. (A23), $f_{\mathbf{k}n}$ is the Fermi-Dirac distribution for the energy eigenvalue $E_{\mathbf{k}n}$. In sum, the Knight shift is given by a weighted sum of orbitally-resolved spin susceptibilities, where the weight is given by the orbital-dependent hyperfine coupling $\lambda^{\rm hf}(\mathbf{R},\tau)$.

In order to obtain the numerical value for $\delta\mathbf{B}^{\rm hf}$, one needs to know $\lambda^{\rm hf}(\mathbf{R},\tau)$. In general, this quantity depends on both $\mathbf{R}$ and τ. For example,

$$\lambda^{\rm hf}({\rm Se_{in}},P2) = 0, \tag{A24}$$

because the $P2$ orbital is odd under spatial inversion about Se_{in}. For Se_{out} and Bi atoms, electronic structure calculations appear to suggest that $\lambda^{\rm hf}(\mathbf{R},P1) \simeq \lambda^{\rm hf}(\mathbf{R},P2)$.

We evaluate Eq. (A23) using a tetragonal lattice regularization of Eq. (A2) and confining the momentum integral to the first Brillouin zone. The lattice constants in the xy plane are $a_x = a_y \simeq 4$ Å, while the lattice constant along the z direction is $a_z \simeq 30$ Å. We find that $\chi_{ij} = \chi_i\delta_{ij}$, so that $K_{ij} = K_i\delta_{ij}$. There is a strong xxz anisotropy of the Knight shift; this is largely inherited from the anisotropy in the g factors. It is convenient to separate the sum over n and n' in Eq. (A23) into an "interband" and an "intraband" part. The interband part contains transitions between the valence and conduction bands and is responsible for the fact that the Knight shift tends to a nonzero value in the limit of vanishing carrier density (i.e., when the Fermi level is inside the bulk gap). Note that this contribution to the Knight shift is *different* from the chemical shift: For one thing, it originates from the hyperfine coupling. The intraband part refers to transitions within the conduction bands or within the valence bands. At times mistakenly identified with the full Knight shift, this contribution is proportional to the density of states at the Fermi energy.

3. Indirect internuclear coupling

In this section, we wish to determine the indirect coupling between different nuclei, which is mediated by the itinerant electrons. The starting point is once again Eq. (A3). Due to the hyperfine interaction, electrons near a nucleus feel the nuclear spin. Because these electrons are itinerant, they communicate the information about that nuclear spin to other nuclei, thereby resulting in an effective internuclear interaction.

The form of this effective internuclear coupling is well known [36]:

$$\mathcal{H}_{\rm ind} = -\frac{1}{2}\sum_{\mathbf{R}\mathbf{R}'}\sum_{\mathbf{k}\mathbf{k}'}\sum_{nn'}\frac{\langle\psi_{\mathbf{k}n}|\mathbf{s}\cdot\mathbf{I}(\mathbf{R})A(\mathbf{r}-\mathbf{R})|\psi_{\mathbf{k}'n'}\rangle\langle\psi_{\mathbf{k}'n'}|\mathbf{s}\cdot\mathbf{I}(\mathbf{R}')A(\mathbf{r}-\mathbf{R}')|\psi_{\mathbf{k}n}\rangle}{E_{\mathbf{k}'n'}-E_{\mathbf{k}n}}(f_{\mathbf{k}n}-f_{\mathbf{k}'n'}), \tag{A25}$$

where all quantities have been defined in the preceding section. Using the contact interaction form for the hyperfine coupling [cf. Eq. (A4)], we obtain

$$\mathcal{H}_{\rm ind} = -\frac{1}{2}\left(\frac{2\mu_0}{3}g_s\mu_B\hbar\right)^2\gamma_R\gamma_{R'}\frac{1}{V^2}\sum_{\mathbf{k}\mathbf{k}'}\sum_{nn'}e^{i(\mathbf{k}-\mathbf{k}')\cdot(\mathbf{R}-\mathbf{R}')}(f_{\mathbf{k}n}-f_{\mathbf{k}'n'})\frac{[u^*_{\mathbf{k}n}(\mathbf{R})\mathbf{s}\cdot\mathbf{I}(\mathbf{R})u_{\mathbf{k}'n'}(\mathbf{R})][u^*_{\mathbf{k}'n'}(\mathbf{R}')\mathbf{s}\cdot\mathbf{I}(\mathbf{R}')u_{\mathbf{k}n}(\mathbf{R}')]}{E_{\mathbf{k}'n'}-E_{\mathbf{k}n}}, \tag{A26}$$

where γ_R and $\gamma_{R'}$ are the nuclear gyromagnetic ratios at sites $\mathbf{R}$ and $\mathbf{R}'$, respectively. Here, we will be interested in the case in which one of the nuclei is Bi and the other is inner Se (Se_{in}). Using $|\langle\mathbf{R}|P1\rangle|^2 \simeq |\langle\mathbf{R}|P2\rangle|^2$ for $\mathbf{R}$ = Bi and $|\langle\mathbf{R}|P2\rangle|^2 \simeq 0$ for $\mathbf{R} = {\rm Se_{in}}$, we obtain

$$H_{\rm ind} = \sum_{\mathbf{R}\mathbf{R}'}\sum_{\alpha\beta}I^\alpha(\mathbf{R})J_{\alpha\beta}(\mathbf{R}-\mathbf{R}')I^\beta(\mathbf{R}') \quad (\alpha,\beta\in\{x,y,z\}), \tag{A27}$$

where

$$J_{\alpha\beta}(\mathbf{R}-\mathbf{R}') = -\tfrac{1}{2}\lambda^{\rm hf}({\rm Bi},P1)\lambda^{\rm hf}({\rm Se_{in}},P1)\gamma_{\rm Bi}\gamma_{\rm Se}\hbar^2\chi_{\alpha\beta}(\mathbf{R}-\mathbf{R}',0) \tag{A28}$$

is the indirect internuclear coupling, $\lambda^{\rm hf}({\rm Bi},P1)$ and $\lambda^{\rm hf}({\rm Se_{in}},P1)$ are the hyperfine couplings defined in Eq. (A22), $\gamma_{\rm Bi}$ and $\gamma_{\rm Se}$ are the respective gyromagnetic ratios, and

$$\chi_{\alpha\beta}(\mathbf{R}-\mathbf{R}',0) = \frac{V_{\rm mol}}{N_A}\int\frac{d^3q}{(2\pi)^3}e^{i\mathbf{q}\cdot(\mathbf{R}-\mathbf{R}')}\chi_{\alpha\beta}(\mathbf{q},0)$$

$$\chi_{\alpha\beta}(\mathbf{q},0) = \mu_B^2g_s^2\frac{V_{\rm mol}}{N_A}\int\frac{d^3k}{(2\pi)^3}\sum_{nn'}(f_{\mathbf{k}n}-f_{\mathbf{k}-\mathbf{q}n'})\frac{\langle u_{\mathbf{k}-\mathbf{q}n'}|s^\alpha(\mathbf{1}+\tau^z)|u_{\mathbf{k}n}\rangle\langle u_{\mathbf{k}n}|s^\beta(\mathbf{1}+\tau^x)|u_{\mathbf{k}-\mathbf{q}n'}\rangle}{E_{\mathbf{k}-\mathbf{q}n'}-E_{\mathbf{k}n}} \tag{A29}$$

are the real-space and momentum-space static susceptibilities of itinerant electrons. The numerical evaluation of Eq. (A28) requires extracting some numerical values for $\lambda^{\rm hf}({\rm Bi}, P1)$ and $\lambda^{\rm hf}({\rm Se_{in}}, P1)$ from experiment. In order to do so, we first evaluate the contact Knight shift for Bi and inner Se, considering only the Fermi-surface (intraband) contribution. This contribution is carrier-density-dependent and vanishes at low temperature if the Fermi level lies inside the bulk gap. Afterwards, we look at the experimental data on how the Knight shift depends on the carrier concentration. For instance, in Bi, the NMR shift is measured to change from 0.3% to 0.7% as the carrier density grows from 0 to 2×10^{19} cm^{-3} [14]. Then, comparing our theory to the measured data, we extract $\lambda^{\rm hf}({\rm Bi}, P1)\mu_B\gamma_{\rm Bi}\hbar \simeq 28$ μeV. For Se, we take $\lambda^{\rm hf}({\rm Se_{in}}, P1)\mu_B\gamma_{\rm Se}\hbar \simeq 7$ μeV, which yields a Knight shift that changes a few hundreds of ppm when the carrier density is increased from 0 to 10^{-19} cm^{-3} (cf. Fig. 4 in the main text). Finally, we input these same values of $\lambda({\rm Bi}, P1)$ and $\lambda({\rm Se_{in}}, P1)$ into our theory of the indirect internuclear coupling. Clearly, it would be desirable to carry out a full first-principles calculation of the indirect internuclear without any phenomenological parameter. This task is outside the scope of this paper and will be tackled elsewhere.

In the expression for the susceptibility, it is instructive to separate the sum over n and n' onto interband and intraband parts. Here, "interband transition" refers to a transition that takes place between the valence band and the conduction band. Transitions between bands that are degenerate in energy at $q = 0$ are counted as "intraband." The intraband transitions contribute to the indirect internuclear coupling only in doped topological insulators, and in fact they lead to the Ruderman-Kittel-Kasuya-Yosida (RKKY) interaction. On the other hand, the interband transitions exist even in the insulating regime and produce the Bloembergen-Rowland (BR) interaction. In doped semiconductors, the RKKY interaction is often believed to be more important than the BR interaction, because the former (latter) decreases as a power law (exponentially) with the internuclear distance. Interestingly, our calculation shows that the interband contribution to the susceptibility strongly dominates over the intraband contribution for experimentally relevant carrier densities. This is partly due to the narrow gap of these insulators, and partly due to the large matrix element of the spin operator between the conduction and valence bands. Consequently, the indirect internuclear coupling is mainly of BR type.

After evaluating Eq. (A28) numerically, we obtain the contribution from the indirect internuclear coupling to the NMR linewidth for an inner Se nucleus:

$$\langle \Delta\omega^2 \rangle = \frac{I(I+1)}{3\hbar^2} \sum_j J_{zz}(\mathbf{R}_i - \mathbf{R}_j)^2, \tag{A30}$$

where $I = 9/2$ is the magnitude of the Bi nuclear spin. It must be noted that J_{xy}, J_{xz}, and J_{yz} are nonzero but small compared to J_{xx}, J_{yy}, and J_{zz}; hence, they will be neglected herein. Besides, there is no significant asymmetry between J_{zz} and J_{xx}, and likewise $J_{xx} = J_{yy}$. The sum over j is evaluated over all the positions of the Bi atoms in the crystal. The reason for restricting the sum to Bi nuclei is that their abundance and spin are much higher than that of Se nuclei. A numerical evaluation of Eq. (A30) leads to Fig. 4 of the main text. The calculated linewidth is weakly dependent on the carrier density at low-to-moderate doping, which reflects the fact that the BR coupling is dominant.

[1] M. Z. Hasan and C. L. Kane, Rev. Mod. Phys. **82**, 3045 (2010).
[2] X.-L. Qi and S.-C. Zhang, Rev. Mod. Phys. **83**, 1057 (2011).
[3] L. Fu and C. L. Kane, Phys. Rev. B **76**, 045302 (2007).
[4] J. E. Moore and L. Balents, Phys. Rev. B **75**, 121306 (2007).
[5] R. Roy, Phys. Rev. B **79**, 195322 (2009).
[6] H. Zhang, C.-X. Liu, X.-L. Qi, X. Dai, Z. Fang, and S.-C. Zhang, Nat. Phys. **5**, 438 (2009).
[7] D. Hsieh, D. Qian, L. Wray, Y. Xia, Y. S. Hor, R. J. Cava, and M. Z. Hasan, Nature (London) **452**, 970 (2008).
[8] Y. Xia, D. Qian, D. Hsieh, L. Wray, A. Pal, H. Lin, A. Bansil, D. Grauer, Y. S. Hor, R. J. Cava, and M. Z. Hasan, Nat. Phys. **5**, 398 (2009).
[9] Y. L. Chen, J. G. Analytis, J.-H. Chu, Z. K. Liu, S.-K. Mo, X. L. Qi, H. J. Zhang, D. H. Lu, X. Dai, Z. Fang, S. C. Zhang, I. R. Fisher, Z. Hussain, and Z.-X. Shen, Science **325**, 178 (2009).
[10] D. Hsieh, Y. Xia, D. Qian, L. Wray, F. Meier, J. H. Dil, J. Osterwalder, L. Patthey, A. V. Fedorov, H. Lin, A. Bansil, D. Grauer, Y. S. Hor, R. J. Cava, and M. Z. Hasan, Phys. Rev. Lett. **103**, 146401 (2009).
[11] Y. S. Hor, A. Richardella, P. Roushan, Y. Xia, J. G. Checkelsky, A. Yazdani, M. Z. Hasan, N. P. Ong, and R. J. Cava, Phys. Rev. B **79**, 195208 (2009).
[12] J. G. Analytis, J.-H. Chu, Y. Chen, F. Corredor, R. D. McDonald, Z. X. Shen, and I. R. Fisher, Phys. Rev. B **81**, 205407 (2010).
[13] Z. Wang, T. Lin, P. Wei, X. Liu, R. Dumas, K. Liu, and J. Shi, Appl. Phys. Lett. **97**, 042112 (2010).
[14] D. M. Nisson, A. P. Dioguardi, P. Klavins, C. H. Lin, K. Shirer, A. C. Shockley, J. Crocker, and N. J. Curro, Phys. Rev. B **87**, 195202 (2013).
[15] Y. S. Hor, A. J. Williams, J. G. Checkelsky, P. Roushan, J. Seo, Q. Xu, H. W. Zandbergen, A. Yazdani, N. P. Ong, and R. J. Cava, Phys. Rev. Lett. **104**, 057001 (2010).
[16] M. Kriener, K. Segawa, Z. Ren, S. Sasaki, and Y. Ando, Phys. Rev. Lett. **106**, 127004 (2011).
[17] T. V. Bay, T. Naka, Y. K. Huang, H. Luigjes, M. S. Golden, and A. de Visser, Phys. Rev. Lett. **108**, 057001 (2012).
[18] B. Zocher and B. Rosenow, Phys. Rev. B **87**, 155138 (2013).
[19] B.-L. Young, Z.-Y. Lai, Z. Xu, A. Yang, G. D. Gu, Z.-H. Pan, T. Valla, G. J. Shu, R. Sankar, and F. C. Chou, Phys. Rev. B **86**, 075137 (2012).
[20] D. M. Nisson, A. P. Dioguardi, X. Peng, D. Yu, and N. J. Curro, Phys. Rev. B **90**, 125121 (2014).
[21] S. Mukhopadhyay, S. Krämer, H. Mayaffre, H. F. Legg, M. Orlita, C. Berthier, M. Horvatić, G. Martinez, M. Potemski, B. A. Piot, A. Materna, G. Strzelecka, and A. Hruban, Phys. Rev. B **91**, 081105 (2015).
[22] R. E. Taylor, B. Leung, M. P. Lake, and L.-S. Bouchard, J. Phys. Chem. C **116**, 17300 (2012).

[23] D. Koumoulis, T. C. Chasapis, R. E. Taylor, M. P. Lake, D. King, N. N. Jarenwattananon, G. A. Fiete, M. G. Kanatzidis, and Louis-S. Bouchard, Phys. Rev. Lett. **110**, 026602 (2013).

[24] D. Koumoulis, B. Leung, T. C. Chasapis, R. Taylor, D. King, M. G. Kanatzidis, and L.-S. Bouchard, Adv. Funct. Mater. **24**, 1519 (2014).

[25] D. Y. Podorozhkin, E. V. Charnaya, A. Antonenko, R. Mukhamad'yarov, V. V. Marchenkov, S. V. Naumov, J. C. A. Huang, H. W. Weber, and A. S. Bugaev, Phys. Solid State **57**, 1741 (2015).

[26] R. Yu, W. Zhang, H.-J. Zhang, S.-C. Zhang, X. Dai, and Z. Fang, Science **329**, 61 (2010).

[27] X. Kou, Y. Fan, M. Lang, P. Upadhyaya, and K. L. Wang, Solid State Commun. **215-216**, 34 (2015).

[28] P. Das, Y. Suzuki, M. Tachiki, and K. Kadowaki, Phys. Rev. B **83**, 220513 (2011).

[29] We have verified that no sample heating occurs during our measurements, despite the sample being the primary heat sink for RF power.

[30] A. Abragam, *The Principles of Nuclear Magnetism* (Oxford University Press, London, UK, 1983).

[31] G. C. Carter, *Metallic Shifts in NMR* (Pergamon Press, Oxford, UK, 1977).

[32] E. Pavarini and I. I. Mazin, Phys. Rev. B **74**, 035115 (2006).

[33] S. Boutin, J. Ramírez-Ruiz, and I. Garate, arXiv:1602.02649 (2016).

[34] N. Bloembergen and T. J. Rowland, Phys. Rev. **97**, 1679 (1955).

[35] C.-X. Liu, X.-L. Qi, H. J. Zhang, X. Dai, Z. Fang, and S.-C. Zhang, Phys. Rev. B **82**, 045122 (2010).

[36] C. H. Ziener, S. Glutsch, and F. Bechstedt, Phys. Rev. B **70**, 075205 (2004).

[37] Preliminary field-dependent ^{77}Se NMR measurements in a $Cu_{0.1}Bi_2Se_3$ single crystal give for $B_0 \parallel c$ slightly smaller field-*independent* linewidths of about 7 kHz (Se_{out}) and 23 kHz (Se_{in}). The field-dependent linewidth for Se_{out} was found to be $\sim$0.6 kHz/T, slightly bigger than in Bi_2Se_3, probably due to distribution of shifts.

[38] While observing the spin echo on Se_{out} with $\tau = 150\ \mu$s, we have inverted also Se_{in} (right after the regular π pulse) for comparison. We found a 10% decrease in echo intensity when both Se were flipped, from which we estimate a decay constant due to Se_{out}-Se_{in} coupling $T_{2G,\text{out-in}} \approx 580\ \mu$s (an order of magnitude shorter than expected from dipolar coupling between Se_{out} and Se_{in}). This effect argues in favor of ^{77}Se -^{77}Se indirect coupling, which is expected to contribute only weakly to the spin echo decay of Se_{out} ($T_{2G,\text{out-out}} \geqslant T_{2G,\text{out-in}}$), since Se_{out} has a smaller hyperfine coupling than Se_{in}.

[39] C. H. Recchia, K. Gorny, and C. H. Pennington, Phys. Rev. B **54**, 4207 (1996).

[40] C. P. Slichter, *Principles of Magnetic Resonance* (Springer-Verlag, New York, 1990).

[41] B. Sapoval and J. Y. Leloup, Phys. Rev. B **7**, 5272 (1973).

[42] We stress that **s** is the bare spin operator, rather than the envelope spin operator (which would be described by a 4×4 matrix and behave as an identity matrix in the orbital space).

[43] We are neglecting the wave-function projection of a *p*-type atomic orbital at the nucleus of a different atom.